The Journal of the Astronautical Sciences (2023) 70:55
https://doi.org/10.1007/s40295-023-00422-7

ORIGINAL ARTICLE

Relative Distance Control of Uncooperative Tethered Debris

Liam Field[1] · **Eleonora M. Botta**[1]

Accepted: 6 November 2023

Abstract

An increasing concern for space-based missions is the potential of collisions with space debris. Long-term mitigation of this risk can be achieved by removing large debris from orbit, as, in particular, collisions involving these can significantly increase the number of smaller debris in orbit. One method of removal involves an active craft capturing and towing a large piece of debris from orbit using a tether. To ensure a successful mission, collisions and tether winding about the target must be avoided. This work proposes relative distance proportional-integral-derivative (PID) and proportional-derivative (PD) controllers to regulate the distance between the chaser and target for a post-capture tethered satellite model. The performances of both controllers are compared to each other and to the performance of an open loop thrust to understand their impact on the system dynamics. The simulation results indicate that PID control is unsuitable for scenarios where the tether is initially slack, as it induces significant angular motion on the target, which could potentially lead to tether winding. However, PD control was found to induce safe angular motion both with an initially slack and an initially taut tether. A sensitivity study found PD control to be robust to the initial chaser-target relative distance and target inertia properties; however, similarly to PID control, it cannot control the angular motion of the target. As such, it is recommended to apply the PD controller after detumbling has been performed or when the debris angular motion is sufficiently small.

Keywords Space debris · Active debris removal · Relative distance control · Sensitivity study · PD control

✉ Eleonora M. Botta
ebotta@buffalo.edu

Liam Field
liamfiel@buffalo.edu

[1] Mechanical and Aerospace Engineering, SUNY University at Buffalo, 211 Bell Hall, Buffalo, NY 14260, USA

Published online: 04 December 2023

1 Introduction

Space debris is a growing operational hazard to space-based missions [1]. The introduction of large constellations and the accelerating number of launches in the coming years is expected to significantly increase the LEO population and further contribute to space debris [2]. To address concerns related to the growth of debris, new regulations have been introduced which restrict the post-mission lifetime of future satellites from the previous standard of 25 years to 5 years [3]. However, a plethora of debris objects that currently populate LEO will remain in orbit for years and will continue to threaten future operations. In particular, collisions between large debris, such as rocket bodies or inactive satellites, are a significant source of debris proliferation across the orbital environment [4]. Such debris objects must be actively disposed of to mitigate the growth of space debris. Promising methods of active debris removal (ADR) involve an active craft (i.e., a chaser) capturing a piece of debris (i.e., the target) through a flexible tether-net [5–9] or tethered harpoon [10–13].

Tethered nets and harpoons provide a means to capture and subsequently tow the target to a disposal orbit. The flexible nature of these systems poses challenges to the control of the chaser-tether-target system. During the towing process, it is necessary to prevent potentially catastrophic events, such as the tether winding about the debris or a chaser-target collision. Aslanov and Yudintsev showed that slackness in the tether is one of the primary contributors to tether winding, indicating that a taut tether is safer for towing the target [14]. Therefore, a certain minimum relative distance, and safe attitude motion of the debris, must be maintained. Jaworski et al. designed a proportional-integral-derivative (PID) controller which could maintain a relative distance and control the target attitude motion [15, 16] via thrust applied to the chaser. Cleary and O'Connor leveraged the robustness of wave-based control to solve the issue of uncertainty in the target parameters [17]. The controller they implemented was able to track a reference velocity while maintaining a relative distance between the chaser and target during a de-orbiting maneuver. A method of debris removal utilizing a chaser-tether-target system was proposed by Trushlyakov and Yudintsev [18], in which a relative distance is maintained by rotating the system about its barycenter. In addition to thrusting, direct control of the tether itself utilizing a reel or winch was proposed by Meng et al. to prevent tether twisting about a debris object in an ADR scenario using an impedance-based tension controller which modified the natural length of the tether [19]. A hierarchical sliding mode controller to command tension in the tether was investigated by Chu et al. for the same purpose [20]. Controls for a configuration of the chaser-tether-target system including sub-tethers, originally proposed by Hovell and Ulrich [21], have also been developed. Shan and Shi have capitalized on the stability of the target attitude in the sub-tether configuration by designing a simple control which actuates based on the relative velocity between the chaser and target [22].

Further development of controls that present a simple option for safely towing the target between burn maneuvers is required. This investigation aims to

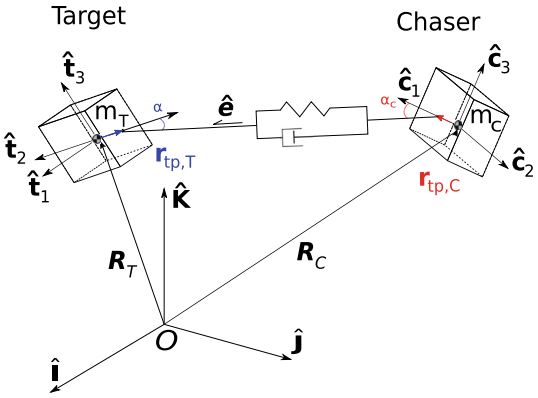

Fig. 1 Chaser, target, and spring-damper tether element with the ECI and body-fixed reference frames

illuminate further the dynamics of the post-capture ADR scenario and propose proportional-derivative (PD) and PID controllers that use thrust to maintain a certain relative distance between the chaser and the target. Their performance at maintaining safe conditions during tethered towing will be analyzed, both in terms of the chaser-target relative distance and of attitude motion of the target.

The remainder of this paper is organized as follows. In Sect. 2, the model of the post-capture ADR system will be discussed. In Sect. 3, control of the chaser's attitude and its relative distance to the target will be introduced. Simulations of the dynamics of the chaser-tether-target system, subject to three different thrust profiles and two initial condition scenarios, will be analyzed in Sect. 4 to determine the success of the controllers at stabilizing the system during the tug. Section 5 will discuss and display the results from a sensitivity study with respect to certain system variables to investigate the robustness of the PD controller when uncertainty is present in the system.

2 System Modeling

A model of the chaser-tether-target system during the post-capture phase is shown in Fig. 1 and described in the following. It consists of two rigid bodies—the chaser and target—as well as a massless tether that is rigidly pinned to both bodies. The target, modeled as a rectangular prism, is a generalization of the bodies that are expected to be removed during ADR missions. The Earth-Centered Inertial frame is defined as $\mathcal{O} = [\hat{\boldsymbol{I}}, \hat{\boldsymbol{J}}, \hat{\boldsymbol{K}}]$, while the chaser and target body-fixed frames are $\mathcal{C} = [\hat{\boldsymbol{c}}_1, \hat{\boldsymbol{c}}_2, \hat{\boldsymbol{c}}_3]$ and $\mathcal{T} = [\hat{\boldsymbol{t}}_1, \hat{\boldsymbol{t}}_2, \hat{\boldsymbol{t}}_3]$, respectively. The target alignment angle, α, is the angle between the tether and the outward facing normal of the side of the target where the tether is attached (which, in this case, is the negative y-axis of the target body-fixed frame, $-\hat{\boldsymbol{t}}_2$). It can be considered a measure of safety since it indicates a potential winding of the tether about the target when it is greater than 90°. For the same purpose, the chaser alignment angle α_c is defined as the angle between the chaser x-axis $\hat{\boldsymbol{c}}_1$ and the tether heading vector.

2.1 Chaser and Target Model

The translational kinematics of the bodies are described in the inertial reference frame by the position $\boldsymbol{R}$ and the velocity $\boldsymbol{V}$ of their centers of mass, where the argument of time has been omitted for improved readability. The angular kinematics are described by an attitude quaternion $\boldsymbol{q}$ and angular velocity vector $\boldsymbol{\omega}$. The attitude quaternion, expressed in the inertial reference frame, is defined as $\boldsymbol{q} = [q_0, q_1, q_2, q_3]^T$ with scalar component q_0 and vector component $[q_1, q_2, q_3]^T$. The angular velocity of a body is expressed in its respective body-fixed frame as $\boldsymbol{\omega} = [\omega_x, \omega_y, \omega_z]^T$. The kinematic relationships are then

$$\dot{\boldsymbol{R}} = \boldsymbol{V} \tag{1}$$

$$\dot{\boldsymbol{q}} = \frac{1}{2}\begin{bmatrix} -q_1 & -q_2 & -q_3 \\ q_0 & -q_3 & q_2 \\ q_3 & q_0 & -q_1 \\ -q_2 & q_1 & q_0 \end{bmatrix}\begin{bmatrix} \omega_x \\ \omega_y \\ \omega_z \end{bmatrix} \tag{2}$$

In this work, the only external forces accounted for are the gravitational attraction of Earth, control inputs, and tether tension. Other external forces and disturbances, such as J_2 effects, solar radiation pressure, and atmospheric drag, would have a noticeable effect on the dynamics over a long duration. However, only a time period of a few hundred seconds in the post-capture phase is considered here, the choice of which will be illustrated in Sect. 4. These assumptions result in the translational dynamic equations for each body given by

$$m\ddot{\boldsymbol{R}} = -m\mu\frac{\boldsymbol{R}}{||\boldsymbol{R}||^3} + \boldsymbol{T} + \boldsymbol{U} \tag{3}$$

where m is the mass of the body, μ is the standard gravitational parameter of Earth, vector $\boldsymbol{T}$ indicates the force from tension, and $\boldsymbol{U}$ is a control force vector. The tension in the tether is presented in detail later, together with the tether modeling. As only the chaser is actively controlled, $\boldsymbol{U}$ is zero for the target; to the control forces acting on the chaser, instead, is dedicated Sect. 3 entirely.

The rotational dynamics of each rigid body are given by

$$\dot{\boldsymbol{\omega}} = J_X^{-1}\left({}^{\mathcal{X}}\boldsymbol{r}_{tp,X} \times {}^{\mathcal{X}}A^{\mathcal{O}}\boldsymbol{T} - \boldsymbol{\omega} \times J_X\boldsymbol{\omega} + \boldsymbol{\tau}\right) \tag{4}$$

where the gravity gradient torque has been ignored considering its small magnitude compared to the moment produced by the tether. Vector ${}^{\mathcal{X}}\boldsymbol{r}_{tp,X}$ denotes the position of the tether attachment point on body X in its respective body-fixed frame $\mathcal{X}$ (e.g., frame $\mathcal{C}$ for the chaser body, C), the principal mass moment of inertia matrix of body X is given by J_X, and the rotation matrix ${}^{\mathcal{X}}A^{\mathcal{O}}$ is required to transform the tension from the inertial to the body-fixed frame. Given that the tether is rigidly connected to both the target and chaser, the tether attachment point position in the body frame ${}^{\mathcal{X}}\boldsymbol{r}_{tp,X}$ is assumed to be constant. Similarly to the translational dynamics, the control torque $\boldsymbol{\tau}$ is zero for the target, and will be addressed for the chaser in Sect. 3.

2.2 Tether Model

The tether is modeled by a single spring-damper element which cannot support compression. The tension force in the tether is therefore calculated as

$$\boldsymbol{T} = \max(T, 0)\hat{\boldsymbol{e}} \tag{5}$$

where the tension magnitude is computed, according to the Kelvin–Voigt model, as $T = k(l - l_0) + c\dot{l}$, where l is the tether length, l_0 is its natural length, and $\dot{l}$ is the length rate of change. The tether parameters k and c represent its stiffness and damping, respectively. The tether mass, calculated using its physical parameters as $m_l = \rho A l_0$ with density ρ and cross-sectional area A, is equally distributed to the target and chaser. In Equation (5), vector $\hat{\boldsymbol{e}}$ is the tether unit heading vector, defined as

$$\hat{\boldsymbol{e}} = \frac{\boldsymbol{R}_T +^{\mathcal{O}} \boldsymbol{r}_{tp,T} - \boldsymbol{R}_C -^{\mathcal{O}} \boldsymbol{r}_{tp,C}}{||\boldsymbol{R}_T +^{\mathcal{O}} \boldsymbol{r}_{tp,T} - \boldsymbol{R}_C -^{\mathcal{O}} \boldsymbol{r}_{tp,C}||} \tag{6}$$

where it should be noted that the denominator of $\hat{\boldsymbol{e}}$ is equivalent to the tether length l. The length rate $\dot{l}$ is found by taking the relative velocity of the tether attachment points on the chaser and target then projecting the resultant vector onto $\hat{\boldsymbol{e}}$, which can be expressed as:

$$\dot{l} = (\boldsymbol{V}_T +^{\mathcal{O}} \boldsymbol{A}^{\mathcal{T}}\boldsymbol{\omega}_T \times^{\mathcal{T}} \boldsymbol{r}_{tp,T} - \boldsymbol{V}_C -^{\mathcal{O}} \boldsymbol{A}^{\mathcal{C}}\boldsymbol{\omega}_C \times^{\mathcal{C}} \boldsymbol{r}_{tp,C}) \cdot \hat{\boldsymbol{e}} \tag{7}$$

3 Chaser Controls

The dynamics of the chaser, and of the entire system by reflection, can be controlled by appropriately defining the control forces $\boldsymbol{U}$ and torques $\boldsymbol{\tau}$, as per the equations of motion (3) and (4). In this Section, controllers for the attitude of the chaser and for its distance relative to the target will be described.

3.1 Attitude

The attitude of the chaser is controlled by a sliding mode controller alike to that derived by Crassidis et al. [23]. The actuators for the chaser attitude control system are thrusters, which are assumed to supply exactly the required input torque about the center of mass of the chaser. The desired attitude quaternion is extracted from a rotation matrix constructed using a set of orthogonal axes as follows: the x-axis of the set is $\hat{\boldsymbol{e}}$; the z-axis is the cross product of $\hat{\boldsymbol{e}}$ and $\boldsymbol{R}_C$; finally, the y-axis completes the right-handed set. This choice of desired axes limits the torque applied by the tether on the chaser and prevents winding of the tether about the chaser. In fact, as long as the x-axis of the set is defined along the tether, the tether torque affecting the chaser will be minimal for any chosen z- or y- axis definition.

3.2 Relative Distance Control

To ensure that the tether remains in tension throughout the dynamics, such that possible collisions or winding of the tether are prevented, a relative distance PID controller is introduced on the chaser craft. This controller uses knowledge of the tether length and length rate to maintain a desired elongation of the tether. The states required to calculate these quantities could be estimated using a combination of LiDAR, tension sensors, and/or camera-based feature tracking, the latter two having been used together in recent work by Bourabah et al. [24]. The actuators on the chaser are its thrusters, which are assumed to act directly on the chaser's center of mass. The thrusters are considered to be continuous and able to perfectly track the required control thrust, while actuator saturation is not considered at this time.

Any control which intends to maintain a chaser-target relative distance must contend with the tension in the tether. The elongation, derived from the relative distance between the tether attachment points on the end bodies, provides a measure of the tension, given the longitudinal dynamics of the system are at steady-state. Therefore, by controlling the elongation, the chaser-target relative distance can be controlled by applying a force counter to the tension. The error variable, based on the tether elongation, for the PID controller, is given by

$$e(t) = \Delta l + l_0 - l(t) \tag{8}$$

where Δl is the desired elongation of the tether. As Δl is directly related to the steady-state elongation maintained by the controller, it should be chosen such that the magnitude of the steady-state tension is small. The input magnitude calculated using the error e is

$$F_{PID}(t) = K_P e(t) + K_I \int_0^t e(\tau)\, d\tau + K_D \dot{e}(t) \tag{9}$$

where the constants K_P, K_I, and K_D are the proportional, integral, and derivative gains, respectively. The direction of thrust is chosen as the negative tether heading vector, $-\hat{\boldsymbol{e}}(t)$, such that the input is applying its full effort to minimizing the error variable:

$$\boldsymbol{F}_{PID}(t) = -F_{PID}(t)\hat{\boldsymbol{e}}(t) \tag{10}$$

The choice of thrusting direction means that, for a positive F_{PID}, the chaser is thrusting away from the target, while for a negative F_{PID} it is thrusting towards it.

As an alternative to PID control, a PD controller is also considered for this work. The PD controller has the same error variable as the PID. The calculated input force magnitude for the PD is then

$$F_{PD}(t) = K_p e(t) + K_d \dot{e}(t) \tag{11}$$

where K_p and K_d are its proportional and derivative gains, respectively. The PD input force $F_{PD}(t)$ is applied in the same direction as that of the PID controller.

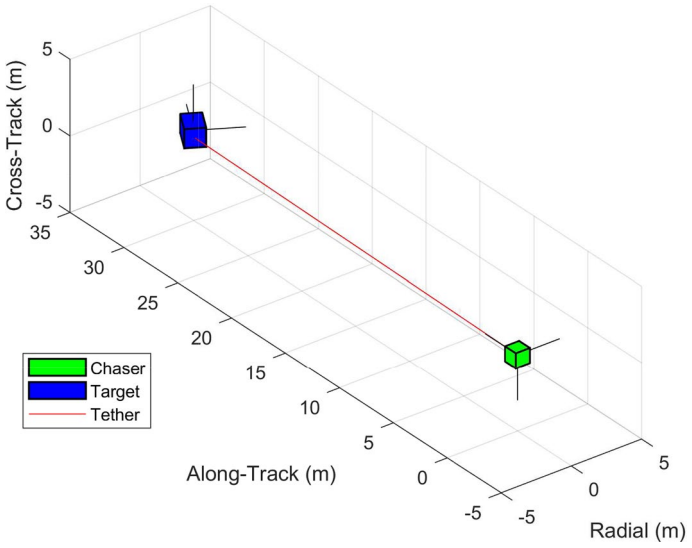

Fig. 2 Snapshot of the system in the chaser LVLH frame at $t = 0$ s

For this work, tuning of the controller gains was performed heuristically over the transient period of the system response to the controllers. Two initial condition scenarios were chosen for the tuning, in which the tether was either slightly slack or slightly taut (by less than the desired elongation). The gain combinations which performed best—in terms of overshoot and settling time of the elongation, as well as of the input thrust magnitude—were then selected for the full simulations.

4 Simulations

The performance of the controllers at maintaining a desired elongation and their impact on the system dynamics is analyzed by simulation of the post-capture ADR scenario. The system dynamics and control are simulated in MATLAB using the *ode45* integrator to advance the dynamics for a duration of 500 s, which was found to be sufficient time for the controls to stabilize the longitudinal dynamics of the tether.[1] Two scenarios are run, where the only difference is the initial elongation of the tether. In the first scenario, the tether is initially slightly taut (with an elongation of 3×10^{-5} m), while the tether is slack by 1 m in the second scenario. For both scenarios, the target has an initial alignment angle of 30° (α in Fig. 1) with the tether, representing a non-ideal capture scenario. To visualize the initial conditions of the simulation, Fig. 2 presents a snapshot of the system at $t = 0$ s for the second scenario (i.e., initially slack tether), where the chaser is shown in green, the target in blue, and the tether in red. The axes are for the

[1] This justifies the absence of additional disturbances in Eq. (3).

Table 1 Initial conditions for initially taut tether scenario

Variable	Value
$\boldsymbol{R}_C$ (m)	$[-6176010.87, -42079.190, 2973766.82]^T$
$\boldsymbol{R}_T$ (m)	$[-6176020.96, -42080.997, 2973743.40]^T$
$\boldsymbol{V}_C$ (m/s)	$[-2457.79535, -4404.28547, -5712.40584]^T$
$\boldsymbol{V}_T$ (m/s)	$[-2457.76467, -4404.28338, -5712.420604]^T$
$\boldsymbol{q}_C$ (–)	$[-0.551521076, 0.667700907, 0.471155309, 0.167369874]^T$
$\boldsymbol{q}_T$ (–)	$[-0.85286853, 0.15038373, -0.08682409, 0.49240388]^T$
$\boldsymbol{\omega}_C$ (°/s)	$[0, 0, 0]^T$
$\boldsymbol{\omega}_T$ (°/s)	$[0, 2.8648, 0]^T$

Table 2 Initial Keplerian elements of the chaser orbit

Variable	Value
Semi-major axis (km)	6871
Eccentricity	0.001
Inclination (°)	60
Right ascension of the ascending node (RAAN,°)	20
Argument of periapsis (°)	90
True anomaly (°)	60

chaser Local-Vertical-Local-Horizontal (LVLH) frame, where the radial direction is along $\boldsymbol{R}_C$, the cross-track direction is along the cross product of $\boldsymbol{R}_C$ and $\boldsymbol{V}_C$, and the along-track direction completes the set. The body axes for both craft are represented by sets of orthogonal black lines centered at their respective centers of mass. In the image, it is clear that the chaser body axes are nearly aligned with the LVLH frame, while the target can be seen to be at an angle with respect to the tether in the orbital plane.

The initial conditions for the initially taut tether scenario in Cartesian coordinates are provided in Table 1. The inertial position and velocity of the chaser correspond to a point on an earth-centered orbit defined by the classical orbital elements in Table 2. The initial conditions for the second scenario can be obtained by moving the chaser 1 m closer to the target along the initial tether direction $\hat{\boldsymbol{e}}$, which can be calculated using the position vectors and attitude quaternions in Table 1. The initial target angular rates are such that the initial rotation of the target is solely about its primary axis $\hat{\boldsymbol{t}}_2$ (i.e., $\omega_y \neq 0, \omega_x = \omega_z = 0$). The system parameters for both cases are reported in Table 3. The parameters and certain initial conditions are the same as in Reference [21], which allowed to validate the dynamics in this work.

A desired elongation Δl of 0.01 m was chosen for both controllers in both scenarios. The controller gains—selected from the tuning process mentioned in Sect. 3, given this Δl—are $K_P = 300$ N/m, $K_I = 300$ N/ms, and $K_D = 2000$ Ns/m for the PID controller and $K_p = 300$ N/m and $K_d = 2000$ Ns/m for the PD controller. An additional simulation is performed for both scenarios (i.e., an initially taut and an

Table 3 System parameters for the simulation scenarios

Parameter	Value
Chaser inertia matrix J_C (kg m^2)	diag (83.3, 83.3, 83.3)
Target inertia matrix J_T (kg m^2)	diag (15,000, 3000, 15,000)
Chaser attachment point ${}^{\mathcal{C}}\boldsymbol{r}_{tp,C}$ (m)	$[0.5, 0, 0]^T$
Target attachment point ${}^{\mathcal{T}}\boldsymbol{r}_{tp,T}$ (m)	$[0, -0.875, 0]^T$
Chaser mass m_C (kg)	500
Target mass m_T (kg)	3000
Tether stiffness k (N/m)	1573
Tether damping c (Ns/m)	16
Tether cross-sectional area A (m^2)	7.8540×10^{-7}
Tether density ρ (kg/m^3)	970
Tether natural length l_0 (m)	30

initially slack tether), in which an open loop thrust with a magnitude of 20 N is applied to the chaser in the negative direction of its velocity:

$$F_{OL}(t) = -20\frac{\boldsymbol{V}_C}{||\boldsymbol{V}_C||}. \tag{12}$$

This constant magnitude thrust acts as a baseline case to which the system responses of the PD and PID controllers can be compared and provides an opportunity to investigate the effect of the thrust direction.

4.1 Initially Taut Tether

The profiles of quantities representative of the dynamics of the system in time for the scenario where the tether is initially taut are reported in Fig. 3. Results produced using the PID controller are represented by solid black lines, while those produced by the open loop and PD controllers are represented by dashed blue and red lines, respectively.

The elongation of the tether, in Fig. 3a, displays significant differences between the PID, PD, and open loop controllers. The elongations produced by both the PID and PD controllers lack the oscillatory behavior present in the open loop system response. For the PID controller, the desired elongation of 0.01 m is reached at about 35 s. The PD controller, instead, is characterized by a steady-state error in the elongation of the tether compared to the desired elongation (which is to be expected); in this simulation, the PD controller settles at a steady-state elongation of 0.0014 m, which is reached in about 4 s. The tension in the tether is plotted in Fig. 3b and is observed to have nearly identical behavior, albeit with a different magnitude, to elongation for each control (as is expected). Figure 3c displays the control thrust magnitudes, allowing the reader to visualize the relationship between the thrust applied to the chaser, the elongation of the tether, and the tension present in the tether.

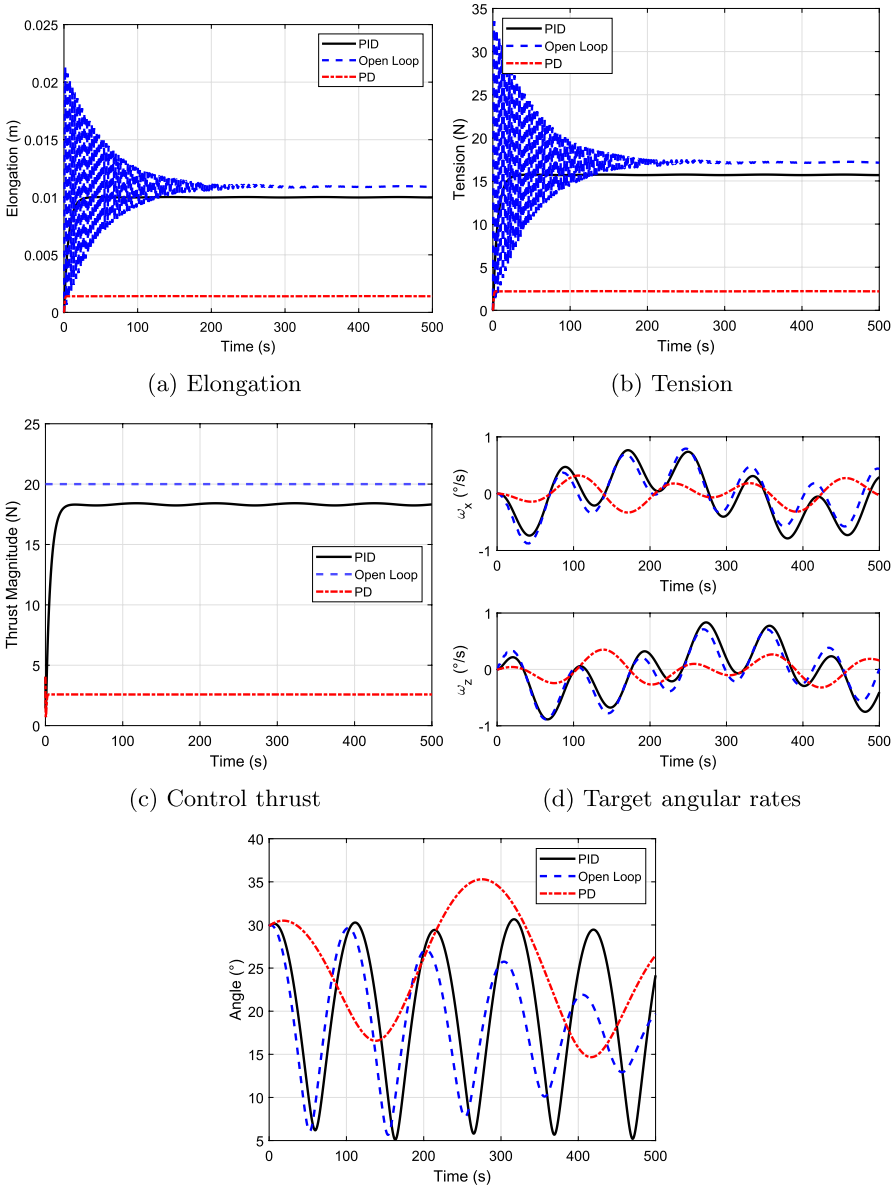

(a) Elongation

(b) Tension

(c) Control thrust

(d) Target angular rates

(e) Tether alignment angle

Fig. 3 Initially taut tether results with PID, PD, and open loop controls

The values of the angular rates of the target about its x- and z-body axes throughout the simulation are shown in Fig. 3d. Here, it should be noted that, due to the choice of the attachment point on the target being along the y-body axis of the target, the angular rate about the y-axis ω_y is unaffected by the tension force and as

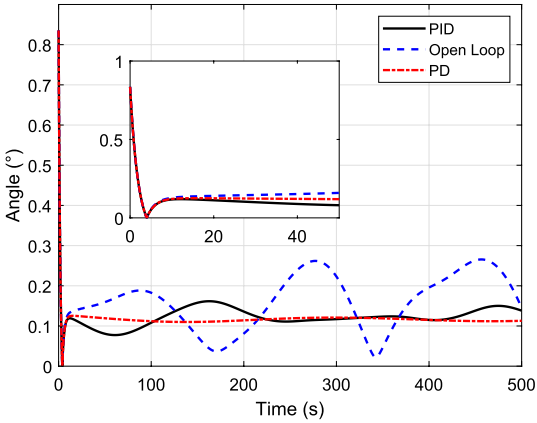

Fig. 4 Chaser alignment angle in initially taut tether simulations

such its plot is omitted. Furthermore, it should be recalled that, in all simulations, the target only rotates about its y-axis initially. From the results in Fig. 3d, it is clear that PD control induces angular rates on the target of lower amplitude compared to both open loop and PID controls. Therefore, the steady-state error that was observed in the elongation actually results in benefits from the point of view of the effect of the control on the target, as milder target rotation leads to a smaller chance of tether winding. The PID and open loop thrusts showcase similar patterns in the angular rates they impart on the target; this is due to the similar levels of thrust (and therefore of elongation and tension in the tether) required by these controllers, which are almost ten times those experienced in the PD-control case (as verified in Fig. 3c).

Figure 3e displays the alignment angles experienced by the target under the three controllers, which are indicative of the likelihood of the tether winding around the target. The alignment angle shows a different mode of oscillation when the chaser is controlled in open loop than either of the other two cases; this is due to the off-tether direction in which the thrust is fired along (i.e., the negative chaser velocity direction). In terms of peak amplitudes, the alignment angles experienced under PID control and open loop control are quite similar; this is expected to be due to the similar thrust levels. However, unlike the open loop controller, the amplitude of the alignment angle does not vary significantly throughout the simulation with PID control. The PD controller is clearly observed to produce a lower frequency and lower amplitude oscillation in the alignment angle, as the lesser tension imparts lower angular momentum to the target.

To display the capability of the chaser attitude controller, Fig. 4 presents the chaser alignment angle, α_c, for each simulation. It is verified that the alignment angle reduces from its initial value, of 0.8°, to almost 0°. After an initial transient period of similar results for the three simulations, the chaser alignment angle values begin to deviate from one another. The PD controller produces non-periodic motion of the lowest amplitude, while oscillations of the greatest amplitude are noticed with open loop control due to its thrusting direction. In all cases, these findings show that the attitude sliding mode controller is capable of maintaining a very small alignment angle, ensuring minimal chance of the tether wrapping the chaser.

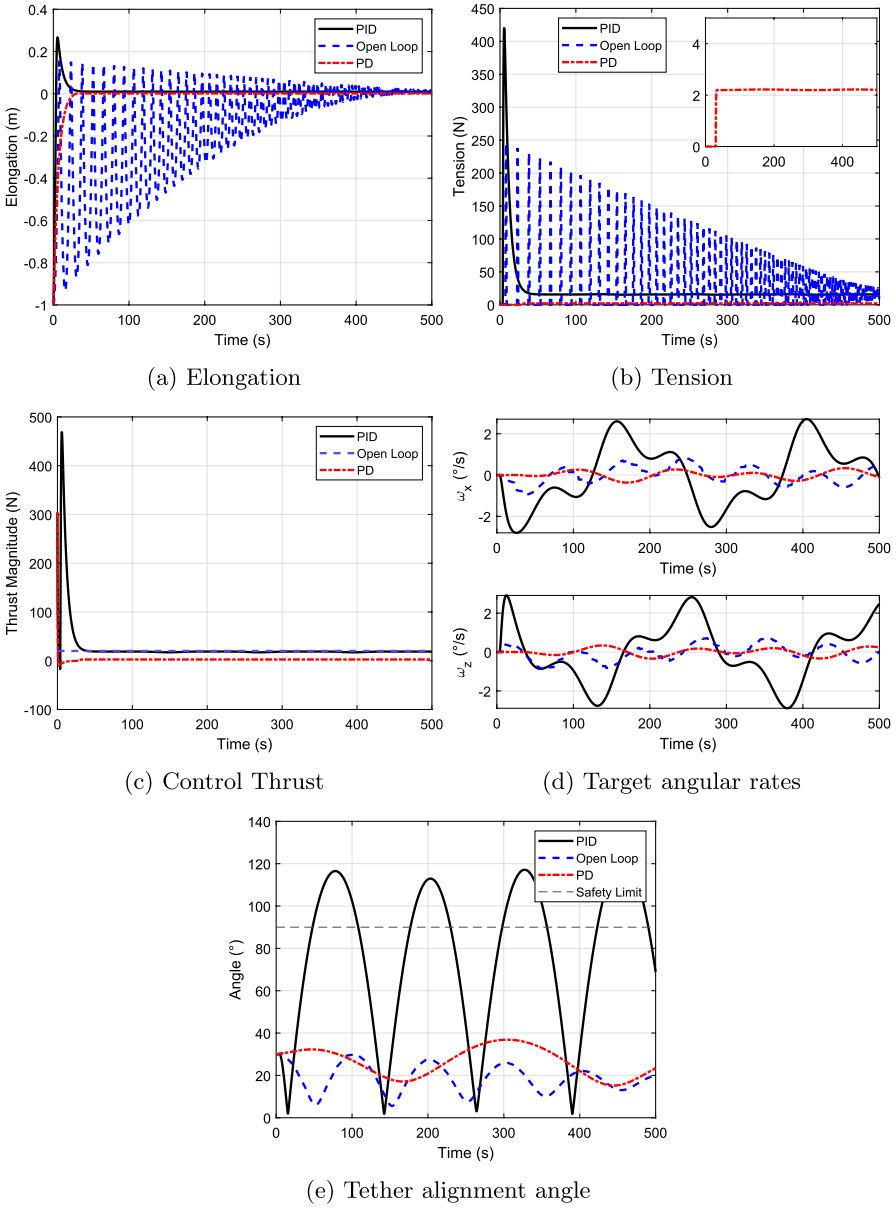

(a) Elongation

(b) Tension

(c) Control Thrust

(d) Target angular rates

(e) Tether alignment angle

Fig. 5 Initially slack tether results with PID, PD, and open loop controls

4.2 Initially Slack Tether

Figure 5 displays the simulation results for the case where the tether is initially in a slack configuration. From the elongation and tension profiles in Fig. 5a, b, it is evident that the responses of the system are substantially different from those

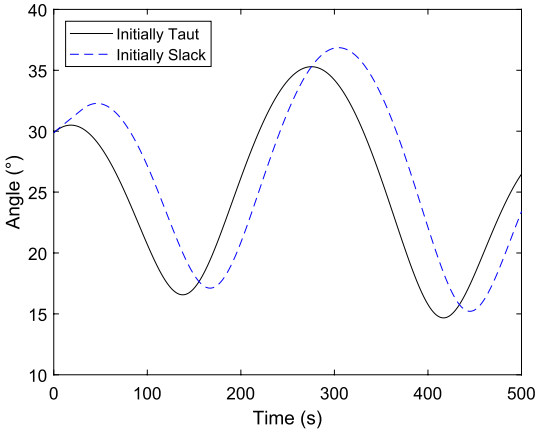

Fig. 6 Comparison of PD control-induced alignment angles for both scenarios

experienced when the tether is initially taut. In particular, the open loop thrust causes significant periods of slackness in the tether, which lead to an inability of the chaser to control the target. In contrast, the significant PID thrust (the magnitude of which is seen in Fig. 5c) is able to quickly bring the tether in an elongated, therefore taut, configuration. At the peak of thrust—which is due to the integral component of the PID, as will be discussed in more detail later—the elongation is significant, of approx. 0.25 m, resulting in tension and stress peaks of approx. 420 N and 0.5348 GPa.[2] After this, the elongation rapidly descends to the desired steady-state value, reaching it at approximately $t = 51$ s. PD control, on the other hand, produces a remarkably similar elongation to the previous scenario, steadying at approx. 0.0014 m.

The angular rates of the target are displayed in Fig. 5d. The angular rates of the open loop and PD controllers are similar in behavior to the previous scenario, with slight differences in their values. Due to the similar behavior in the angular rates, the tether alignment angles caused by the PD and open loop thrusts, which are reported in Fig. 5e, are also similar to the previous scenario. For reference, Fig. 6 directly compares the alignment angles generated by the PD controller for both of the simulated scenarios; it can be seen that the alignment angle behavior is overall similar, with small differences in magnitude and peak angle times. The steady-state thrust produced by the PD controller is approximately the same (at 2.5 N) in both scenarios, indicating that the primary driver of the disparity between the two cases is a result of the later time at which the tether becomes taut in the slack tether scenario (i.e., $t = 30$ s), as the exact torque the tension imparts on the target is different due to the initial tumbling motion of the target.

The significant elongation produced by the PID-regulated thrust causes an angular impulse on the target that is much larger than that due to the other two

[2] It should be noted that this is below the ultimate tensile strength of commercially available 1 mm polymer cords for heavy duty daily uses.

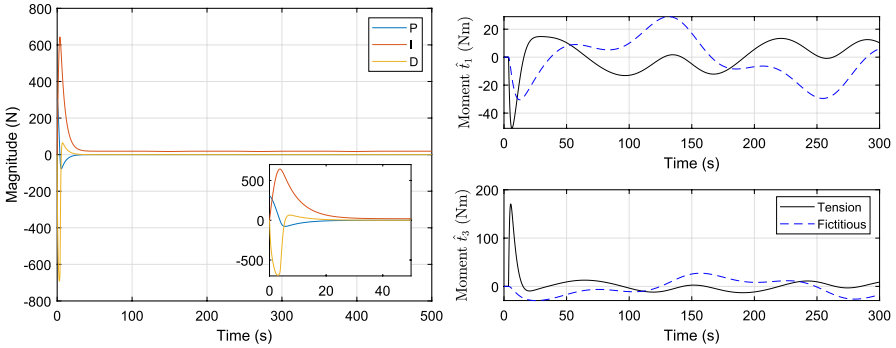

(a) PID thrust components (b) Moments on the target

Fig. 7 Results from the initially slack tether scenario with PID control: (**a**) proportional, integral, and derivative contributions to $F_{PID}(t)$ and (**b**) moments affecting the target in its body-fixed frame

controllers. As a result, the angular rates induced by the PID thrusting are also much larger than those caused by both the PD and the open loop controller. In fact, it is found that PID control induces angular motion of the target that is dangerous to the safety of the ADR mission, as is indicated by the alignment angle. In Fig. 5e, the tether alignment angle is seen to exceed the safety limit of 90°, which is indicated with a dashed black line. This dangerous behavior, initially induced by the high tension in the tether, is ultimately due to the decrease in the thrust generated by the PID controller after the tether becomes taut (which can be appreciated in Fig. 5c), which occurs from the time when the elongation is at its peak until the desired elongation is reached, thereby resulting in a relaxation of the tension. This relaxation causes an inability of the moment applied by the tension to counter the angular impulse produced when the tether first becomes taut.

To further analyze the results of PID control in the scenario when the tether is taut, Fig. 7 reports more quantities of interest. Figure 7a depicts the proportional, integral, and derivative contributions of the PID-controlled thrust in blue, red, and yellow respectively, for the purpose of analyzing the reason for the large peak elongation caused by PID control (see Fig. 5a). It can be seen that the integral component of the control is only increasing while the tether is slack. The resulting thrust imparts significant linear momentum on the chaser, causing the aforementioned large elongation of the tether. Figure 7b displays the moments applied by the tension about the $\hat{\boldsymbol{t}}_1$ and $\hat{\boldsymbol{t}}_3$ axes of the target in the case of PID control and those of the fictitious moment, i.e., $-\boldsymbol{\omega} \times J_X \boldsymbol{\omega}$ from Eq. (4). From this plot, it is confirmed that, once the tether is taut, the moments about $\hat{\boldsymbol{t}}_1$ and $\hat{\boldsymbol{t}}_3$ due to the tension are greater in magnitude than the fictitious moments about the same axes. However, by $t = 15$ s, the elongation has reduced to around 75% of its peak value, and the magnitude of the moment on the target due to the tension has similarly decreased. As the tether relaxes further, reaching its steady-state tension at $t = 51s$, the magnitudes of both the applied and fictitious moments begin to oscillate about similar values.

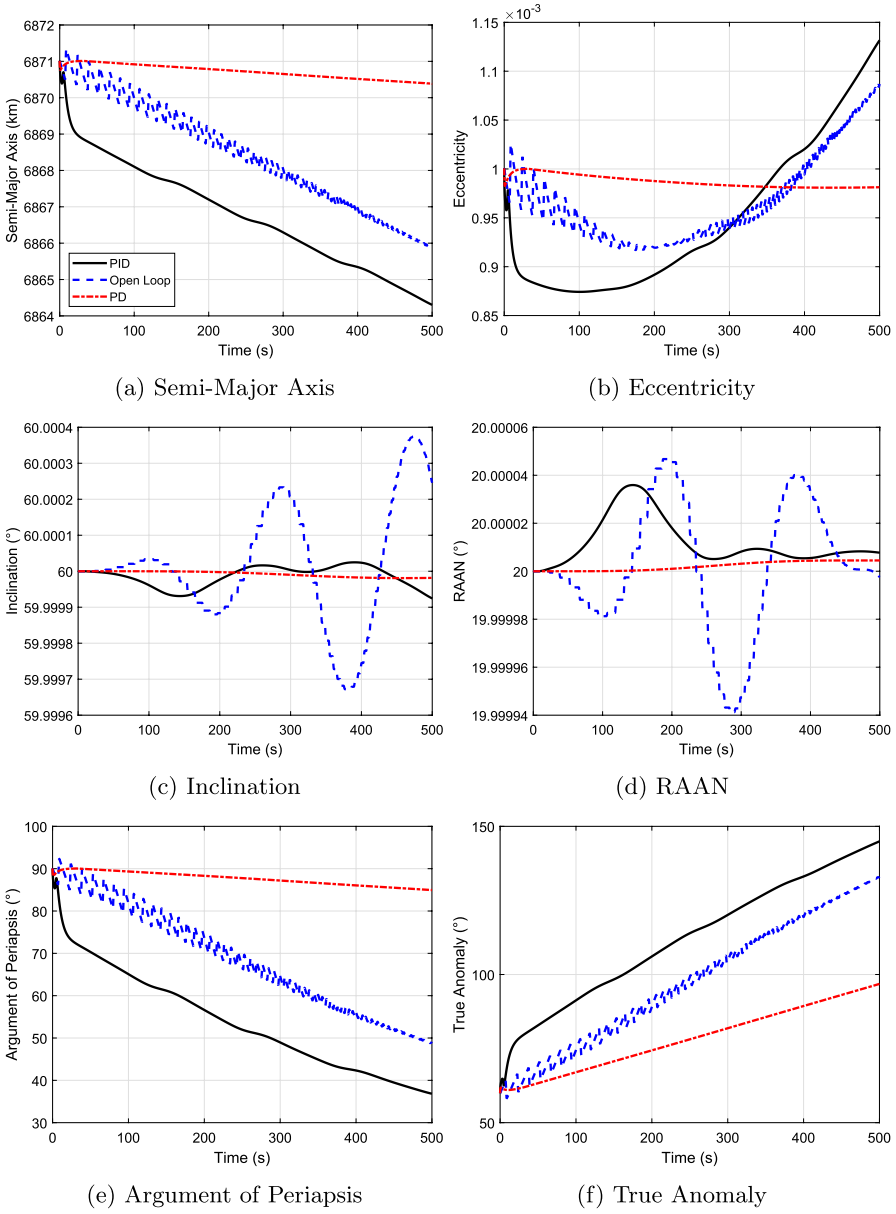

(a) Semi-Major Axis (b) Eccentricity

(c) Inclination (d) RAAN

(e) Argument of Periapsis (f) True Anomaly

Fig. 8 Orbital elements of the chaser for each simulation in the initially slack tether case

The classical orbital elements for the chaser[3] in simulation with each control are given in Fig. 8. As would be expected due to the smaller thrust it applies, the PD

[3] The target is excluded due to the close proximity between it and the chaser.

control causes slower orbital changes compared to the other two controls. The large thrust applied by the PID control in the first 20 s of simulation, instead, directly causes the large initial element changes visible in Fig. 8a, b and e, f. For all controls, the changes in the semi-major axis and eccentricity indicate that the perigee is decreasing. Among all the simulations, the maximum orders of magnitude of the deviations from the initial inclination and RAAN are of 10^{-4} deg and 10^{-5} deg, respectively, indicating there is negligible out-of-plane variation (see Fig. 8c, e). Clearly, all the controls have a notable effect on some of the orbital parameters of the chaser.

4.3 Discussion

Overall, the results of simulating the dynamics of the chaser-tether-target system with PID control showed that this controller is able to achieve the desired elongation, but at the cost of causing dangerous target attitude motion if the tether is initially slack. By removing the integrator component (i.e., with PD control), however, the safety of the induced angular motion on the target can be recovered even in the initially slack tether scenario. The fact that the desired elongation is not exactly achieved with PD control is not as critical as ensuring the safe towing of a target debris object.

It is expected from these results that the PD controller would always induce less angular motion on the target given non-ideal initial conditions (i.e., when the tether alignment angle is non-zero, and the tether is slack by a significant amount). In fact, the PD controller will always result in preferable system behavior compared to the PID controller, as the integral component of the PID will always cause a larger thrust. Consequentially, the propellant consumption of the PID control would be larger than that of the PD control. As the exact post-capture system states will not be known before capture, the ability of the PD controller to behave in similar ways given different initial elongation scenarios is highly favorable. To confirm this notion and to further investigate the capabilities of the PD controller, a sensitivity study in which the target properties and initial conditions are varied across a range of possible values is presented in the following.

5 Sensitivity Study of PD Control

The small set of solutions that were presented in Sect. 4 do not fully represent the possible scenarios that could be encountered during a removal mission. In addition, uncertainty is intrinsic to an ADR mission, such that the robustness of the PD relative distance controller to uncertainties in the target parameters and system initial conditions needs to be analyzed. To this end, a sensitivity study of the system is conducted to understand how the controller performs given variations of a few key variables. For each variable, reasonable error bounds are first determined. Then, an array of the concerned variable is created in one of two ways depending on whether the variable is considered to be affected by measurements taken by the chaser or to

Table 4 Nominal conditions of sensitivity study

Parameter	Value
$\boldsymbol{R}_T$ (m)	$[-6176021.31, -420810.61, 2973742.56]^T$
$\boldsymbol{q}_T$ (–)	$[0.86272974, 0.07548105, 0.21131016, -0.45315341]^T$

be intrinsic to the target. The array for the first type of variable is built by randomly sampling from a Gaussian distribution where the error bounds are treated as 3σ bounds and the mean is determined by the nominal conditions, while for the second type of variable a uniform distribution between the bounds is used.

The variables for the sensitivity study are chosen based on their impact on the system dynamics and their propensity for uncertainty in the ADR scenario. For example, the chaser and tether properties are not included in the study, as it is safe to assume those would be known a priori. Properties intrinsic to the target such as its mass, mass moments of inertia, and initial angular rates, as well as the here considered measured initial chaser-target relative distance and tether attachment point on the target, each play a significant role in determining the dynamics of the system. They also have some inherent uncertainty from the perspective of the chaser and of mission planners. In particular, the properties of the target are the most likely to be unknown and they exist irrespective of the chaser's sensory array. While the mass distribution in the target determines its moments of inertia, performing a sensitivity study where mass variations affect the inertia would make it difficult to discern the impact each variable has on the system dynamics. If this relationship was considered, the geometry of the target would have to change to keep the moments of inertia the same, further complicating the study. For simplicity and ease of analysis, this relationship is ignored, such that the mass and moments of inertia of the target may be varied independently. Furthermore, the components of the angular rates and the mass moments of inertia are varied independently from one another. However, the $x-$ and $z-$ components of the target tether attachment point, ${}^{\mathcal{T}}\boldsymbol{r}_{tp,T}$, are varied simultaneously, with each assumed to be independently Gaussian distributed.

In performing the sensitivity study, nominal conditions to which the variations in the variables should be compared are needed. For this study, the nominal conditions are very similar to the initially slack tether scenario from Sect. 4, except for the initial tether alignment angle, which is changed to 0° (see Table 4 for the initial states that differ as a result of this modification). This change was necessary as the significant initial alignment angle of 30° may impact the conclusions drawn from the results of the other variables, and the PD controller was already shown to be safe with this angle. However, the initial relative distance along the tether direction remains the same as the initially slack scenario (i.e., 29 m between the attachment points). Considering that the state of tension would be recognizable by the chaser craft and that it should be avoided during capture, it is unlikely for the capture

Table 5 Error bounds for variables part of the sensitivity study

Variable	Error bound
Target mass	±300 kg
Target inertia matrix	± diag[3000 600 3000] kgm^2
Target angular rates	±2.292°/s
Initial relative distance	±0.3 m
Target attachment point components	±0.25 m

process to result in a positive elongation, indicating that the choice of nominal relative distance is suitable. For the target attachment point study, however, the relative distance is kept at the nominal value while the alignment angle is permitted to vary along with the attachment point. This follows from the fact that imperfect knowledge of the attachment point would, from the perspective of the chaser, precipitate error in the alignment angle.

The error bounds for each variable are tabulated in Table 5. They are chosen based on experimental data where possible, based on the RemoveDEBRIS mission [8]; otherwise, the bounds are determined arbitrarily to test the capabilities of the controller. The bounds for the angular rates were chosen to be lower than the nominal value of ω_y (i.e., 2.86 °/s)—as that axis is considered the primary spin axis—but still large enough to present a significant deviation from the nominal conditions. For the initial relative distance along the tether, the error is chosen as 0.3 m due to the similarity in the target shapes from this study and the RemoveDEBRIS mission [8]. The bounds for the target attachment point components are chosen such that the distribution of points lies within a circle of radius 0.25 m on the $-y$ face of the target. The number of samples for the intrinsic and measured variables is 20; the simulation time for each of the simulations is set to 500 s.

Due to the complicated nature of the dynamics, the controller performance itself, and safety considerations, the outputs of the sensitivity study are threefold. To understand the sensitivity of the angular dynamics of the target to the variables, the squared norm of the angular velocity integrated over the simulation, denoted as W, is used, as this provides a scalar for which a higher value indicates more significant angular motion:

$$W(t) = \int_0^t ||\boldsymbol{\omega}(\tau)||^2 d\tau. \tag{13}$$

The controller performance is evaluated by the control effort, E_c, which indicates the challenge in controlling the system. It is calculated as the integral of the absolute value of the control force magnitude F_{PD}:

$$E_c(t) = \int_0^t |F_{PD}(\tau)| d\tau. \tag{14}$$

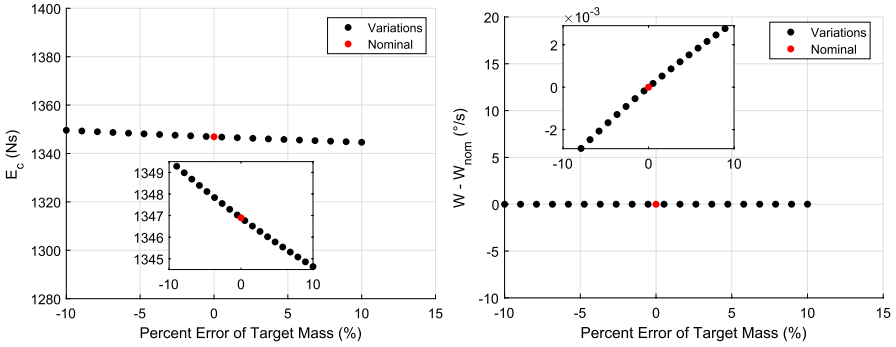

(a) Control Effort (b) Angular Rate Integral

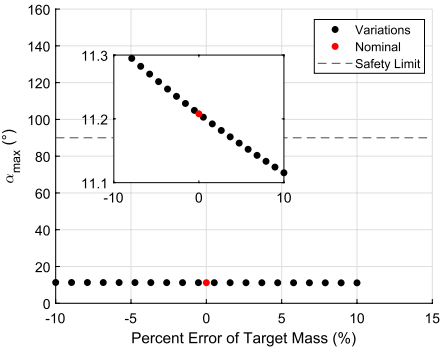

(c) Peak Alignment Angle

Fig. 9 Outputs from varying the target mass

Finally, the peak alignment angle α_{max} achieved over the course of a simulation is used to determine if the mission was safe. The following sections will report and discuss the results of the sensitivity study, demarcated by the variable of interest, in terms of the above-described measures: W, E_c, and α_{max}. The reader should note that, in order to ease comparison of the impact of the different variables, the y-axes of the plots for a given measure are the same across the sensitivity studies.

5.1 Target Mass Study

The effects of varying the target mass are analyzed through the outputs depicted in Fig. 9, where each black marker represents a non-nominal simulation and the red marker is the output relative to the nominal condition. The control effort in Fig. 9a indicates small variations with respect to the nominal conditions. A lower target mass requires a greater thrust as the target is more responsive to the tension in the tether when its mass is lower, requiring the chaser to continue maneuvering away from the target to maintain the desired relative distance. Figure 9c displays the peak alignment angle, which exhibits a similar trend as the control effort, and remains

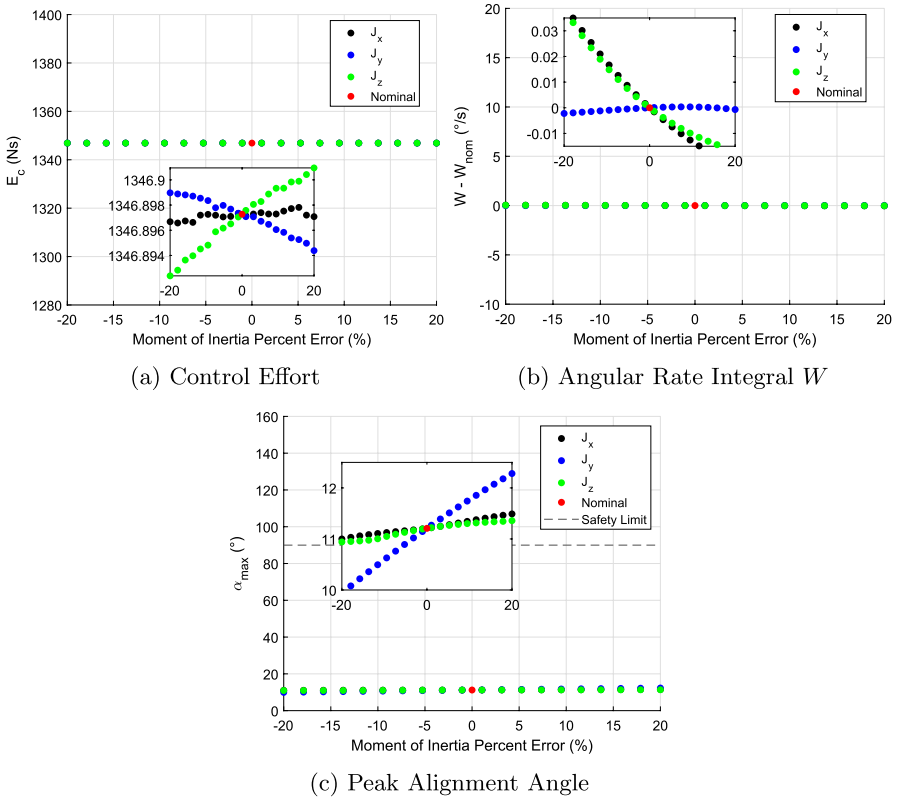

(a) Control Effort

(b) Angular Rate Integral W

(c) Peak Alignment Angle

Fig. 10 Outputs from varying the target moments of inertia

well below the safety limit of 90° in all simulations. However, with increased mass, the value of the angular rate integral W, shown in Fig. 9b as the difference between it and the nominal angular rate integral W_{nom}, increases slightly, with a maximum deviation from the nominal of 0.0027 °/s. Considering that the control effort and W are integrated for the entire simulation, it should be noted that the differences between the variations and the nominal conditions are marginal, indicating that the controller is capable of dealing with variations in the target mass at least up to 10% of the nominal.

5.2 Target Moments of Inertia Study

The outputs from varying each of the principal moments of inertia are reported together in Fig. 10, where the black, blue, and green markers represent the outputs from variations in J_x, J_y, and J_z, respectively, again with a red marker indicating the nominal output. From the plots, it is clear that variations in J_x and J_z result in similar trends. This is explained by the initial symmetry of the target body axes with respect to the tether, which is aligned with the target y-axis. From Fig. 10a, it is seen that

increasing J_y decreases the control effort, albeit only slightly, which is opposed to the trend for the mass moments of inertia about the other two axes. A reason for this is that when J_y is varied, $\dot{\omega}_y$ remains zero due to the symmetry of the target's moments of inertia about the other axes. This is not the case when varying J_x and J_z, where $\dot{\omega}_y$ is nonzero due to coupling in the angular dynamics. Such differences in dynamics would affect the angular rates and subsequently the tether length rate of change $\dot{l}$, which the controller requires to calculate a thrust. In any case, it can be concluded that the controller requires a small change in thrust to account for the variations, as the order of the differences from the nominal control effort are on the scale of 10^{-2} Ns. The angular rate integral in Fig. 10b shows that varying J_y has a smaller effect on the angular motion, compared to variations in J_x and J_z. Again, this is most likely due to a nonzero $\dot{\omega}_y$ which alters the dynamics from the nominal case when $J_x = J_z$. Compared to the other two outputs, different behavior occurs in the peak alignment angle (see Fig. 10c), where all the variations display a positive trend, with J_y having a maximum difference from the nominal of about 1.2°, while J_x and J_z have a maximum difference of about 0.2° for the simulated sampled conditions. While these differences are not significant, they are sufficient to conclude that when $J_x = J_z$ there is greater transverse motion of the target center of mass with respect to the tether.

5.3 Target Initial Angular Rates Study

The time-integral of the squared norm of the angular rate vector, the control effort, and the peak alignment angle obtained for variations in the angular rates ω_x, ω_y, and ω_z are reported in Fig. 11 with associated markers colored black, blue and green, respectively. The outputs obtained in the nominal conditions for ω_x and ω_z (i.e., 0 °/s) and for ω_y (i.e., 2.8648 °/s) are indicated with red markers. Similar to what was observed with the moments of inertia, there are two general trends in the outputs: quadratic behaviors in E_c and W for ω_x and ω_z, and linear relationships for ω_y. The peak alignment angle behavior for ω_x and ω_z, however, appears more similar to a notch. The symmetry in the nominal moments of inertia J_x and J_z results in similar magnitude angular rate components about those target axes, causing the quadratic trend (for example, see the angular rate components for PD control in Fig. 3d, where both ω_x and ω_z can be seen to have a maximum magnitude of around 0.25 °/s).

From Fig. 11 it is clear that varying the initial angular rates ω_x and ω_z significantly impacts each of the outputs. Instead, while varying ω_y alters W significantly—due to ω_y remaining constant throughout the simulation—(see Fig. 11b), the control effort is barely affected (see Fig. 11a). This is due to the fact that—compared to varying ω_x and ω_z—varying ω_y causes the inertial velocity of the target attachment point (and the associated tether length rate of change $\dot{l}$), to be smaller across each simulation as a consequence of smaller ω_x and ω_z amplitudes. Further evidence of this can be found in the peak alignment angles in Fig. 11c: increasing the initial ω_x and ω_z magnitude has a substantial effect on the alignment angle, to the point that the safety limit is exceeded in some cases, as the motion of the target center of mass

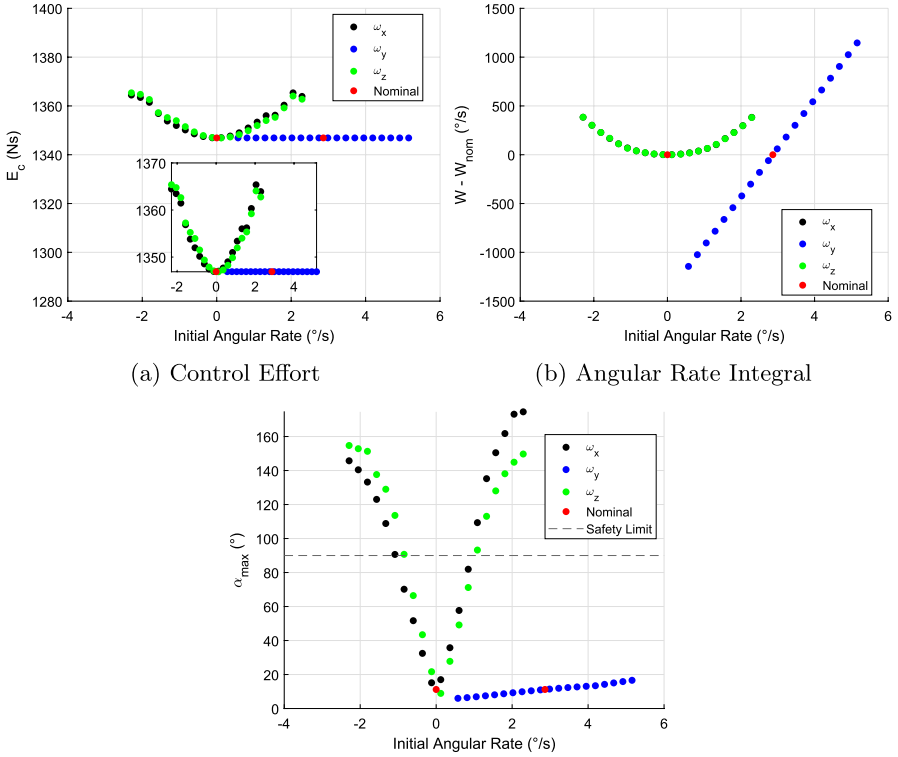

(a) Control Effort

(b) Angular Rate Integral

(c) Peak Alignment Angle

Fig. 11 Outputs from varying the target angular rates

relative to the target attachment point is increased. Safety, however, is not impacted by varying ω_y.

5.4 Chaser-Target Relative Distance Study

Figure 12 presents the results of varying the initial relative distance between the chaser and target, where a positive percent error means the chaser is farther from the target. The control effort (seen in Fig. 12a) shows a significant linear decrease with the error, which is to be expected given the definition of the process variable e for the PD controller, as less thrust is commanded when the chaser is farther away from the target. Both the peak alignment angle α_{max} and the angular rate integral W increase slightly when the relative distance increases, and the maximum deviations from the nominal α_{max} and W are of 0.16° and 0.018 °/s, respectively. As was discussed in Sect. 4.2, this is due primarily to the time at which the tether becomes taut. The varying pose of the target across these times, which are all within 10 s of each other, causes marginal differences in the applied moment of the tether on the

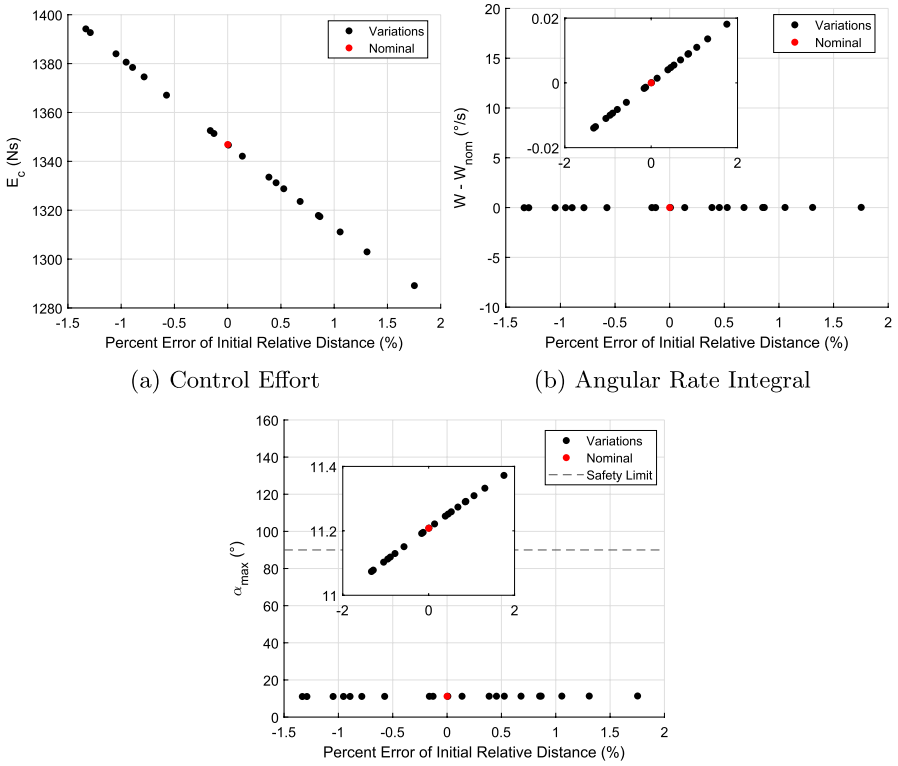

(a) Control Effort

(b) Angular Rate Integral

(c) Peak Alignment Angle

Fig. 12 Outputs from varying the initial chaser-target relative distance

target, thereby altering the target angular rates and, therefore, the alignment angle compared to the nominal.

5.5 Target Attachment Point Study

The sensitivity study outputs from the variation of the $x-$ and $z-$components of the target attachment point position are given in Fig. 13, where the horizontal axes of the plots is a function of the distance between the nominal and non-nominal tether attachment points, $d = ||^{\mathcal{T}}\boldsymbol{r}_{tp,n} - {}^{\mathcal{T}}\boldsymbol{r}_{tp,v}||_2$. Similarly to varying J_x and J_z from Sect. 5.2, displacing the tether attachment point from the y-axis of the target causes the tension to produce a moment about this axis and, as a consequence, introduces non-zero $\dot{\boldsymbol{\omega}}_y$. In Fig. 13a, two trends can be appreciated in the control effort: one positive and the other negative, differentiated by the sign of the $z-$component of the attachment point position. Due to the initial conditions, if $z > 0$ the initial attachment point moves towards the chaser, while if $z < 0$ the attachment point moves away from it; this has a slight impact on the length rate of change (of approx. 10^{-4} m/s), marginally affecting the relative dynamics and subsequently producing the

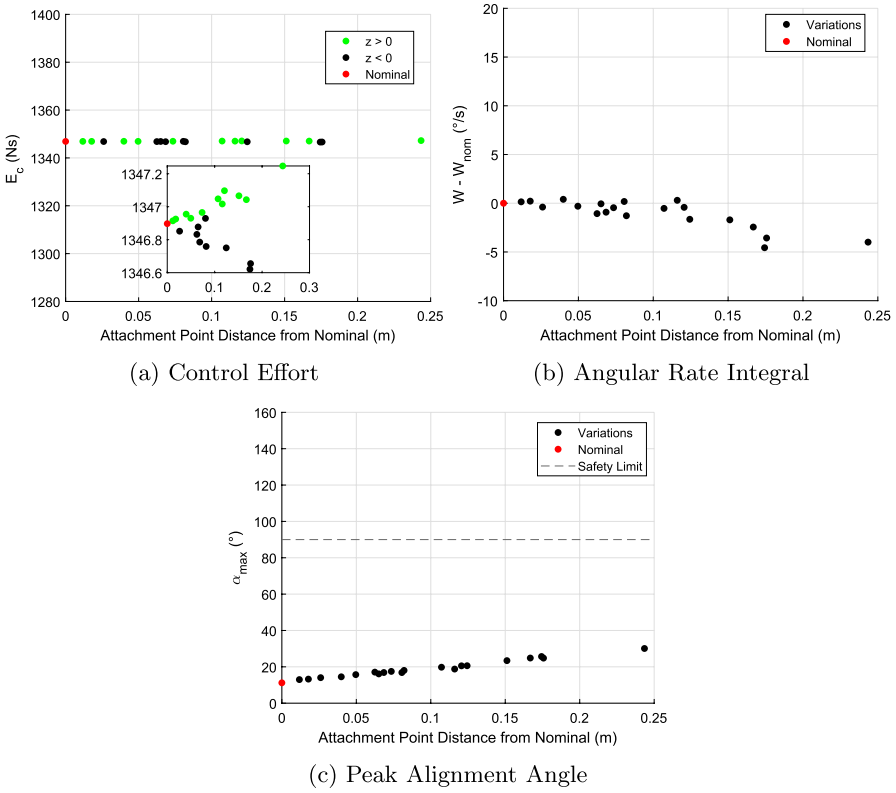

(a) Control Effort

(b) Angular Rate Integral

(c) Peak Alignment Angle

Fig. 13 Outputs from varying the tether attachment point on the target

trends displayed in the control effort after 500 s. In contrast, the angular rate integral and the peak alignment angle in Fig. 13b, c each display only one clear trend. The trends are opposite to each other, such that, broadly, the integral decreases as the peak alignment angle increases, a relationship that was also observed in Sects. 5.1 and 5.2. The positive trend of the peak alignment angle is expected, as the initial angle increases with d by definition. Overall, the results indicate that the PD control can handle non-nominal tether attachment point positions on the target, since their effect is contained and peak alignment angles remain well below the safety threshold.

5.6 Discussion

The sensitivity studies showed that the PD controller is capable of maintaining safe operation in a number of non-nominal conditions. In particular, the PD controller is capable of dealing with a range of target inertia properties and uncertainty in the initial relative distance and tether attachment point position on the target. However, dangerous dynamics can be introduced given sufficient initial angular rate

magnitudes about the target $x-$ or $z-$ axes, due to the choice of the nominal tether attachment point. While not unexpected, this limits the application of the PD controller to missions in which the target angular rates are suitable or in which detumbling is carried out in the immediate post-capture phase. Furthermore, in a single mission, we might expect multiple of these uncertainties to exist simultaneously, possibly compounding their individual effects and resulting in undesired outcomes.

6 Conclusion

In this work, PID and PD controllers were proposed to regulate the distance between the chaser and the target in the post-capture phase of a tethered ADR mission. The performance of both controllers was compared to each other and to that of open loop control to understand the impact of different control strategies on the dynamics of the system. Situations in which the tether was initially taut and initially slack were analyzed.

The PID controller was confirmed to be capable of achieving the desired relative distance between the chaser and the target. However, in the absence of saturation and under certain initial conditions, the angular motion it induced on the target indicated that the tether could wind around the target, jeopardizing the safety, and therefore the success, of the debris removal mission. On the other hand, PD control was found to induce angular motion of smaller amplitude on the target, allowing the system to remain within the limits for safety in both simulated scenarios. In fact, the angular motion of the target was found to be very similar in both simulations under PD control, despite the initial chaser-target relative distance difference.

A sensitivity study was then performed on the PD controller, and it was found that the controller is robust to uncertainties in the target inertia properties, initial relative distance, and the tether attachment point on the target. However, the results of the sensitivity study also reinforced the notion that the PD relative distance controller is unable to directly command the angular motion of the target; as a result, for certain initial angular rates, the alignment angle reached values exceeding the safety limit. Based on this investigation, the use cases of the relative-distance PD controller are limited by the uncertainties in the angular rates of the target. It is recommended that this controller be utilized after detumbling the target or when the debris angular motion is mild, in order to avoid a potential mission-ending scenario. It should be noted that the sensitivity studies that led to this conclusion only account for a small subset of the potential parameter space for this system. Specifically, the compound effects of the variables and the influence of additional parameters (e.g., target shape and associated internal mass distribution, initial system orientation) remain to be investigated.

Acknowledgements This work was funded by the National Science Foundation (NSF), under the CMMI Program, Award number 2105011. Liam Field acknowledges reception of the NASA Space Grant Fellowship.

Data availability Not applicable.

Declarations

Conflict of interest The authors have no conflicts of interest to declare that are relevant to the content of this article.

References

1. Liou, J.-C., Johnson, N.L.: Instability of the present LEO satellite populations. Adv. Space Res. **41**(7), 1046–1053 (2008). https://doi.org/10.1016/j.asr.2007.04.081
2. Murtaza, A., Pirzada, S.J.H., Xu, T., Jianwei, L.: Orbital debris threat for space sustainability and way forward. IEEE Access **8**, 61000–61019 (2020). https://doi.org/10.1109/ACCESS.2020.2979505
3. Space Innovation IB Docket No. 22-271 Mitigation of Orbital Debris in the New Space Age IB Docket No. 18-313, FCC 22-74 (2022)
4. Liou, J.-C., Johnson, N.L., Hill, N.: Controlling the growth of future LEO debris populations with active debris removal. Acta Astronaut. **66**(5–6), 648–653 (2010). https://doi.org/10.1016/j.actaastro.2009.08.005
5. Botta, E.M., Sharf, I., Misra, A.K., Teichmann, M.: On the simulation of tether-nets for space debris capture with vortex dynamics. Acta Astronaut. **123**, 91–102 (2016). https://doi.org/10.1016/j.actaastro.2016.02.012
6. Botta, E.M.: Deployment and Capture Dynamics of Tether-Nets for Active Space Debris Removal. Thesis, McGill University (2017)
7. Sharf, I., Thomsen, B., Botta, E.M., Misra, A.K.: Experiments and simulation of a net closing mechanism for tether-net capture of space debris. Acta Astronaut. **139**, 332–343 (2017). https://doi.org/10.1016/j.actaastro.2017.07.026
8. Aglietti, G.S., et al.: The active space debris removal mission RemoveDebris. Part 2: in orbit operations. Acta Astronaut. **168**, 310–322 (2020). https://doi.org/10.1016/j.actaastro.2019.09.001
9. Ru, M., Zhan, Y., Cheng, B., Zhang, Y.: Capture dynamics and control of a flexible net for space debris removal. Aerospace **9**(6), 299 (2022). https://doi.org/10.3390/aerospace9060299
10. Aslanov, V.S., Yudintsev, V.V.: Behavior of tethered debris with flexible appendages. Acta Astronaut. **104**(1), 91–98 (2014). https://doi.org/10.1016/j.actaastro.2014.07.028
11. Sizov, D.A., Aslanov, V.S.: Space debris removal with harpoon assistance: choice of parameters and optimization. J. Guid. Control. Dyn. **44**(4), 767–778 (2020). https://doi.org/10.2514/1.G005484
12. Zhao, W., Pang, Z., Zhao, Z., Du, Z., Zhu, W.: A Simulation and an Experimental Study of Space Harpoon Low-Velocity Impact. Anchored Debris. Materials **15**(14), 5041 (2022). https://doi.org/10.3390/ma15145041
13. Tamaki, Y., Tanaka, H.: Experimental study on penetration characteristics of metal harpoons with various tip shapes for capturing space debris. Adv. Space Res. (2022). https://doi.org/10.1016/j.asr.2022.04.056
14. Aslanov, V.S., Yudintsev, V.V.: Dynamics of large debris connected to space tug by a tether. J. Guid. Control. Dyn. **36**(6), 1654–1660 (2013). https://doi.org/10.2514/1.60976
15. Jaworski, P., Lappas, V., Tsourdos, A., Gray, I., Schaub, H.: Debris rotation analysis during tethered towing for active debris removal. J. Guid. Control. Dyn. **40**(7), 1769–1778 (2017). https://doi.org/10.2514/1.G002390
16. Peters, T.V., et al.: Attitude control analysis of tethered de-orbiting. Acta Astronaut. **146**, 316–331 (2018). https://doi.org/10.1016/j.actaastro.2018.03.016
17. Cleary, S., O'Connor, W.J.: Control of space debris using an elastic tether and wave-based control. J. Guid. Control. Dyn. **39**(6), 1392–1406 (2016). https://doi.org/10.2514/1.G001624
18. Trushlyakov, V.I., Yudintsev, V.V.: Rotary space tether system for active debris removal. J. Guid. Control. Dyn. **43**(2), 354–364 (2020). https://doi.org/10.2514/1.G004615
19. Meng, Z., Wang, B., Huang, P.: Twist suppression method of tethered towing for spinning space debris. J. Aerosp. Eng. **30**(4), 04017012 (2017). https://doi.org/10.1061/(ASCE)AS.1943-5525.0000708
20. Chu, Z., Di, J., Cui, J.: Hybrid tension control method for tethered satellite systems during large tumbling space debris removal. Acta Astronaut. **152**, 611–623 (2018). https://doi.org/10.1016/j.actaastro.2018.09.016

21. Hovell, K., Ulrich, S.: Attitude stabilization of an uncooperative spacecraft in an orbital environment using visco-elastic tethers. In: AIAA Guidance, Navigation, and Control Conference (2016). https://doi.org/10.2514/6.2016-0641
22. Shan, M., Shi, L.: Velocity-based detumbling strategy for a post-capture tethered net system. Adv. Space Res. **70**(5), 1336–1350 (2022). https://doi.org/10.1016/j.asr.2022.06.012
23. Crassidis, J.L., Vadali, S.R., Markley, F.L.: Optimal variable-structure control tracking of spacecraft maneuvers. J. Guid. Control. Dyn. **23**(3), 564–566 (2000). https://doi.org/10.2514/2.4568
24. Bourabah, D., Field, L., Botta, E.M.: Estimation of uncooperative space debris inertial parameters after tether capture. Acta Astronaut. **202**, 909–926 (2023). https://doi.org/10.1016/j.actaastro.2022.07.041